

Figure 1. (a) Schematic illustration showing molecular structural transformation from the cumulene to a diyne moiety. (b) STM image of the self-assembled structure of C_4Br_4 molecules on Au(111). The individual C_4Br_4 molecules are highlighted by dog-bone-shaped contours. (c) Close-up STM image of the C_4Br_4 self-assembled structure overlaid with the DFT-relaxed model. The dark blue dotted lines represent the halogen bonds. (d) Laplace-filtered nc-AFM image allowing the identification of the cumulene skeleton of the C_4Br_4 molecule as indicated by a red arrow. (e) STM image of the same area in (b) after applying STM manipulation. (f, g) Close-up STM image and the Laplace-filtered nc-AFM image of the resulting C_4Br_2 molecules overlaid with the DFT-relaxed model and the chemical structure, respectively. (h–j) High-resolution STM image, corresponding nc-AFM image, and DFT-optimized model of the C_4Br_4 molecule. The experimental and theoretical values of the bond lengths of three consecutive double bonds are shown in (i) and (j), respectively. (k–m) High-resolution STM image, corresponding nc-AFM image, and DFT-optimized model of the C_4Br_2 product. The experimental and theoretical values of bromine-to-bromine distances are shown in (l) and (m), respectively. Scale bars: 2 Å. Scanning parameters: $V_t = -1$ V, $I_t = 0.2$ nA.

the molecule appears as a homogeneous line with little internal contrast²⁵ (as indicated by the red arrow) in the nc-AFM image (Figure 1d). To explore the possibility of carbon skeleton rearrangement from a cumulene to a diyne moiety, an STM manipulation is performed at 4.3 K. To do so, the STM tip is positioned at the site marked “X” in Figure 1b, and then a voltage pulse (2 V) was applied. The subsequently obtained STM image (Figure 1e) shows a local variation (highlighted by a green rectangle) in comparison with the ordered self-assembled structure (Figure 1b). It is clearly seen that two molecules within that region have changed in shape from dog bone to rod, indicating that the molecules undergo a chemical transformation. From the close-up STM image together with the overlaid DFT model (Figure 1f), we attribute the rod-shape molecules to C_4Br_2 , i.e., a partially debrominated product of C_4Br_4 . The corresponding nc-AFM image (Figure

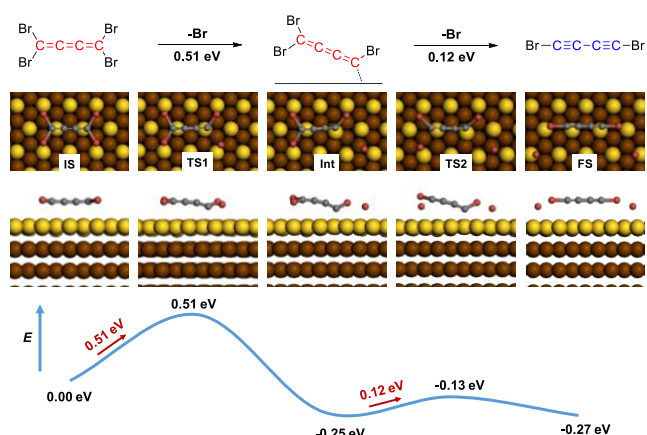


Figure 2. DFT-calculated reaction pathway for the successive C–Br bond activations from different carbon atoms of the C_4Br_4 molecule accompanied by carbon skeleton rearrangement from a cumulene to a diyne moiety on Au(111). The structural models of the initial (IS), transition (TS), intermediate (Int), and final states (FS) along the pathway are also shown.

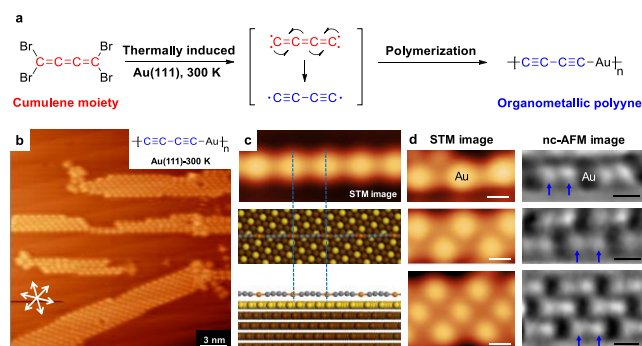


Figure 3. (a) Schematic illustration showing the polymerization from a cumulene moiety to an organometallic polyne. (b) STM image showing the formation of organometallic chains on the Au(111) surface by heating up the sample precovered with C_4Br_4 molecules to 300 K. (c) Equally scaled high-resolution STM image and the corresponding DFT-optimized model of a single organometallic polyne on Au(111). (d) Close-up STM images and the Laplace-filtered nc-AFM images of the single chain, double chain, and triple chain, respectively, in which the diyne moieties within these chains are identified from the nc-AFM images as indicated by blue arrows. Scale bars: 3.8 Å. Scanning parameters: $V_t = -1$ V, $I_t = 0.2$ nA.

1g) shows that the carbon skeleton of the C_4Br_2 molecule is no longer uniform; instead, two separate characteristic protrusions (as indicated by two blue arrows) that were previously known and assigned to two adjacent C–C triple bonds^{28,35,36} are unambiguously imaged. We perform electron density calculations to further understand the observed image contrasts of the cumulene and diyne structures, as shown in Figure S1. The experimental and theoretical values of the bond length for the cumulene moiety of C_4Br_4 are shown in Figure 1i and j, as well as bromine-to-bromine distance for C_4Br_2 in Figure 1l and m. A good agreement is achieved by comparing the measured and calculated values (cf. Table S1). Based on the above information, we conclude that breaking two C–Br bonds results in the transformation from cumulene to diyne. Another data set of tip-induced formation of C_4Br_2 molecules is shown in Figure S2 to demonstrate the reproducibility.

To unravel the underlying mechanism of the skeleton rearrangement in the above-mentioned reaction, we then

perform DFT calculations to explore the possible pathway from the cumulene skeleton of C_4Br_4 to the diyne one of C_4Br_2 on the Au(111) surface, as shown in Figure 2. The energy barrier for cleaving the first C–Br bond is determined to be 0.51 eV, and the second debromination is energetically more favorable from the other terminal carbon atom (0.12 eV) than from the same one (0.48 eV) (cf. Figure S3), respectively. More importantly, it is evidenced that the subsequent carbon skeleton rearrangement is spontaneous. A step further, if four C–Br bonds are entirely cleaved from the C_4Br_4 molecule (Figure S4a), interestingly, the intermediate (C_4 species) strongly interacts with the substrate by pulling out two Au atoms and forms an organometallic structure (Figure S4b), while the chemical structure (i.e., $Au=C=C=C=C=Au$ or $Au-C\equiv C-C\equiv C-Au$) of such a carbon species remains elusive.³⁷ It thus would be of general interest to experimentally reveal the precise chemical bonding configuration of the carbon skeleton involving C_4 in an extended 1-D system.

It was previously demonstrated by Xu and co-workers that both C–Br bonds of the alkenyl *gem*-dibromide group (i.e., $=CBr_2$) could be activated at room temperature on the Au(111) surface.²⁵ Therefore, to obtain the entirely debrominated intermediate of C_4Br_4 , a thermal treatment (by heating the sample precovered with C_4Br_4 molecules to 300 K) is performed, which leads to the formation of ribbon structures composed of individual molecular chains as shown in Figure 3a,b. Interestingly, such a chain structure resembles the previously reported Cu-incorporated organometallic carbon chains (i.e., Cu-carbyne).¹⁹ From the high-resolution STM image and DFT-relaxed structural model (Figure 3c), we then assign the formed chain structure to Au-incorporated organometallic carbon chains (i.e., Au-carbyne), and the bright protrusions within the chain are in relation to the electronic density of states of Au atoms. As also known, debrominated alkenyl *gem*-dibromide groups ($=CBr_2$) directly coupled into the cumulene structure on the Au(111) surface,²⁵ while debrominated alkynyl bromide groups ($\equiv CBr$) form an organometallic structure.³³ Therefore, we suggest that upon entire debromination, the cumulene moiety transforms to the diyne one and then polymerizes into organometallic carbon chains (i.e., organometallic polyynes), which is experimentally confirmed by the nc-AFM images (Figure 3d), where two discrete characteristic protrusions corresponding to two adjacent C–C triple bonds are resolved.^{28,35,36} In addition, a good agreement is also achieved by comparing the experimentally measured bond lengths and the corresponding theoretical values of the organometallic polyyn chain (cf. Table S1). The formation energy of the organometallic chain with respect to the C_4Br_2 molecules are studied with DFT (Figure S5), revealing that the formation of organometallic polyynes from C_4Br_2 molecules and Au adatoms is an exothermic process.

The dI/dV spectra taken at locations of the Au atom and the diyne moiety of an organometallic polyyn are compared to that acquired on the metal substrate. And we assign the increased electronic density at -1.5 and 0.5 V to the valence band maximum (VBM) and conduction band minimum (CBM), respectively, which corresponds to a semiconducting feature (Figure 4a). The subtracted spectra (Figure S6) with detailed discussions are shown in the SI. In addition, the dI/dV line mapping recorded across a single chain, as indicated by the arrow marked in the STM image (Figure 4b, upper panel), reveals that the two electronic states (Figure 4b, lower panel)

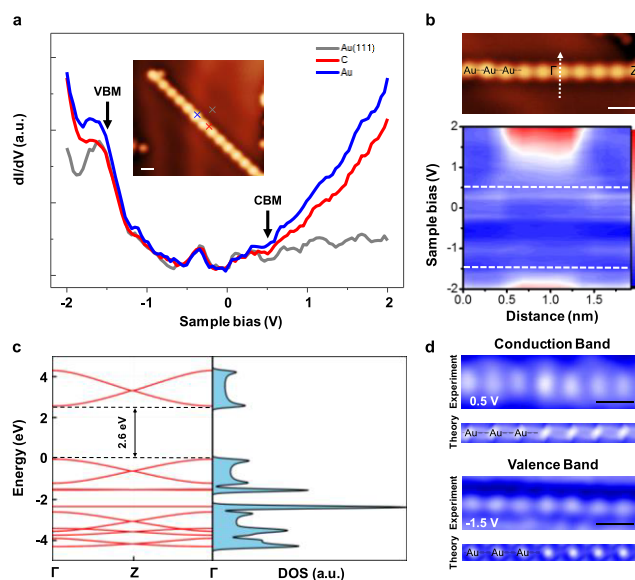


Figure 4. (a) dI/dV spectra taken on the location of the Au atom (blue curve) and the diyne moiety (red curve) of a single organometallic polyyn, and the corresponding positions are marked by blue and red crosses, respectively, as shown in the inset STM image. The gray curve (taken on the position marked by the gray cross) was recorded on the Au(111) surface showing Shockley states at ~ -0.4 V. (b) dI/dV line map taken across a single organometallic polyyn as indicated by the arrow marked in the STM image. The two dashed lines indicate the CBM and VBM, respectively. (c) Calculated band structure (left, red) and DOS (right, blue) of a free-standing organometallic polyyn. The valence band maximum is set at 0 eV. The real-space vector is along the backbone of the chain. (d) Experimental dI/dV maps and the corresponding simulated dI/dV maps at 0.5 V and -1.5 V for the organometallic polyyn. Scale bars: 1 nm.

are concentrated on the chain. We then conducted DFT calculations on the band structure and DOS to study the intrinsic electronic properties of the free-standing organometallic polyyn as shown in Figure 4c, and a semiconducting characteristic with a bandgap about ~ 2.6 eV is obtained. Both the experimental and simulated dI/dV maps along the chain acquired at the CBM and VBM indicate that the electronic density of states are more localized in the proximity of Au atoms (Figure 4d).

We have demonstrated the chemical bond-scission-induced carbon skeleton rearrangement from a cumulene moiety to a diyne one. Although Peierls transition is in principle applied to a truly extended polyyn chain,⁶ the present result shows that the formation of a semiconducting organometallic polyyn with alternating single and triple C–C bonds is achieved, implying that Peierls transition may occur in a rationally designed molecular system with limited length. Moreover, surface-supported metal-incorporated carbon chains would render opportunities for further experimental studies on the characterization of structural and electronic properties with respect to the intrinsic 1-D atomic carbon chain.

■ ASSOCIATED CONTENT

Supporting Information

The Supporting Information is available free of charge at <https://pubs.acs.org/doi/10.1021/jacs.0c01925>.

Experimental details, additional STM image (PDF)

■ AUTHOR INFORMATION

Corresponding Authors

Wei Xu – Interdisciplinary Materials Research Center, College of Materials Science and Engineering, Tongji University, Shanghai 201804, People's Republic of China; orcid.org/0000-0003-0216-794X; Email: xuwei@tongji.edu.cn

Mengxi Liu – CAS Key Laboratory of Standardization and Measurement for Nanotechnology, CAS Center for Excellence in Nanoscience, National Center for Nanoscience and Technology, Beijing 100190, People's Republic of China; orcid.org/0000-0001-7009-5269; Email: liumx@nanoctr.cn

Authors

Xin Yu – Interdisciplinary Materials Research Center, College of Materials Science and Engineering, Tongji University, Shanghai 201804, People's Republic of China

Xin Li – CAS Key Laboratory of Standardization and Measurement for Nanotechnology, CAS Center for Excellence in Nanoscience, National Center for Nanoscience and Technology, Beijing 100190, People's Republic of China; University of Chinese Academy of Sciences, Beijing 100049, People's Republic of China

Haiping Lin – Institute of Functional Nano & Soft Materials (FUNSOM), Jiangsu Key Laboratory for Carbon-Based Functional Materials & Devices, Joint International Research Laboratory of Carbon-Based Functional Materials and Devices, Soochow University, Suzhou 215123, Jiangsu, People's Republic of China; orcid.org/0000-0002-9948-7060

Liangliang Cai – Interdisciplinary Materials Research Center, College of Materials Science and Engineering, Tongji University, Shanghai 201804, People's Republic of China

Xia Qiu – CAS Key Laboratory of Standardization and Measurement for Nanotechnology, CAS Center for Excellence in Nanoscience, National Center for Nanoscience and Technology, Beijing 100190, People's Republic of China; University of Chinese Academy of Sciences, Beijing 100049, People's Republic of China

Dandan Yang – Department of Chemistry, State University of New York, Stony Brook, New York 11794-3400, United States

Xing Fan – Institute of Functional Nano & Soft Materials (FUNSOM), Jiangsu Key Laboratory for Carbon-Based Functional Materials & Devices, Joint International Research Laboratory of Carbon-Based Functional Materials and Devices, Soochow University, Suzhou 215123, Jiangsu, People's Republic of China

Xiaohui Qiu – CAS Key Laboratory of Standardization and Measurement for Nanotechnology, CAS Center for Excellence in Nanoscience, National Center for Nanoscience and Technology, Beijing 100190, People's Republic of China; University of Chinese Academy of Sciences, Beijing 100049, People's Republic of China

Complete contact information is available at:

<https://pubs.acs.org/10.1021/jacs.0c01925>

Author Contributions

*X. Yu, X. Li, and H. Lin contributed equally.

Notes

The authors declare no competing financial interest.

■ ACKNOWLEDGMENTS

The authors thank Prof. Nancy S. Goroff for supporting the organic synthesis of the C₄Br₄ molecule. The authors

acknowledge the financial support from the National Natural Science Foundation of China (21622307, 21790351, 21790353, 21972032, 21721002, 21425310), the Fundamental Research Funds for the Central Universities, the Ministry of Science and Technology of China (2017YFA0205000, 2016YFA0200700), and the Strategic Priority Research Program of Chinese Academy of Sciences (XDB36000000).

■ REFERENCES

- (1) Hayatsu, R.; Scott, R. G.; Studier, M. H.; Lewis, R. S.; Anders, E. Carbynes in Meteorites: Detection, Low-Temperature Origin, and Implications for Interstellar Molecules. *Science* **1980**, *209*, 1515–1518.
- (2) Chalifoux, W. A.; Tykwinski, R. R. Synthesis of Polyyenes to Model the sp-Carbon Allotrope Carbyne. *Nat. Chem.* **2010**, *2*, 967–971.
- (3) Shi, L.; Rohringer, P.; Suenaga, K.; Niimi, Y.; Kotakoski, J.; Meyer, J. C.; Peterlik, H.; Wanko, M.; Cahangirov, S.; Rubio, A.; Lapin, Z. J.; Novotny, L.; Ayala, P.; Pichler, T. Confined Linear Carbon Chains as a Route to Bulk Carbyne. *Nat. Mater.* **2016**, *15*, 634–639.
- (4) Heimann, R. B.; Kleiman, J.; Salansky, N. M. A Unified Structural Approach to Linear Carbon Polytypes. *Nature* **1983**, *306*, 164–167.
- (5) Kennedy, T.; Lieb, E. H. Proof of the Peierls Instability in One Dimension. *Phys. Rev. Lett.* **1987**, *59*, 1309–1312.
- (6) Kertesz, M.; Koller, J.; Azman, A. Ab initio Hartree-Fock Crystal Orbital Studies. II. Energy Bands of an Infinite Carbon Chain. *J. Chem. Phys.* **1978**, *68*, 2779–2782.
- (7) Cahangirov, S.; Topsakal, M.; Ciraci, S. Long-Range Interactions in Carbon Atomic Chains. *Phys. Rev. B: Condens. Matter Mater. Phys.* **2010**, *82*, 195444.
- (8) Liu, M.; Artyukhov, V. I.; Lee, H.; Xu, F.; Yakobson, B. I. Carbyne from First Principles: Chain of C Atoms, a Nanorod or a Nanorope. *ACS Nano* **2013**, *7*, 10075–10082.
- (9) Artyukhov, V. I.; Liu, M.; Yakobson, B. I. Mechanically Induced Metal-Insulator Transition in Carbyne. *Nano Lett.* **2014**, *14*, 4224–4229.
- (10) Cretu, O.; Botello-Mendez, A. R.; Janowska, I.; Pham-Huu, C.; Charlier, J.-C.; Banhart, F. Electrical Transport Measured in Atomic Carbon Chains. *Nano Lett.* **2013**, *13*, 3487–3493.
- (11) Torre, A. L.; Botello-Mendez, A.; Baaziz, W.; Charlier, J.-C.; Banhart, F. Strain-Induced Metal-Semiconductor Transition Observed in Atomic Carbon Chains. *Nat. Commun.* **2015**, *6*, 6636.
- (12) Casillas, G.; Mayoral, A.; Liu, M.; Ponce, A.; Artyukhov, V. I.; Yakobson, B. I.; Jose-Yacamán, M. New Insights into the Properties and Interactions of Carbon Chains as Revealed by HRTEM and DFT Analysis. *Carbon* **2014**, *66*, 436–441.
- (13) Jin, C.; Lan, H.; Peng, L.; Suenaga, K.; Iijima, S. Deriving Carbon Atomic Chains from Graphene. *Phys. Rev. Lett.* **2009**, *102*, 205501.
- (14) Lin, Y.-C.; Morishita, S.; Koshino, M.; Yeh, C.-H.; Teng, P.-Y.; Chiu, P.-W.; Sawada, H.; Suenaga, K. Unexpected Huge Dimerization Ratio in One-Dimensional Carbon Atomic Chains. *Nano Lett.* **2017**, *17*, 494–500.
- (15) Jones, R. O.; Seifert, G. Structure and Bonding in Carbon Clusters C₁₄ to C₂₄: Chains, Rings, Bowls, Plates, and Cages. *Phys. Rev. Lett.* **1997**, *79*, 443.
- (16) Wang, S.; Sun, Q.; Gröning, O.; Widmer, R.; Pignedoli, C. A.; Cai, L.; Yu, X.; Yuan, B.; Li, C.; Ju, H.; Zhu, J.; Ruffieux, P.; Fasel, R.; Xu, W. On-Surface Synthesis and Characterization of Individual Polyacetylene Chains. *Nat. Chem.* **2019**, *11*, 924–936.
- (17) Sun, Q.; Zhang, R.; Qiu, J.; Liu, R.; Xu, W. On-Surface Synthesis of Carbon Nanostructures. *Adv. Mater.* **2018**, *30*, 1705630.
- (18) Talirz, L.; Ruffieux, P.; Fasel, R. On-Surface Synthesis of Atomically Precise Graphene Nanoribbons. *Adv. Mater.* **2016**, *28*, 6222–6231.

- (19) Sun, Q.; Cai, L.; Wang, S.; Widmer, R.; Ju, H.; Zhu, J.; Li, L.; He, Y.; Ruffieux, P.; Fasel, R.; Xu, W. Bottom-Up Synthesis of Metalated Carbyne. *J. Am. Chem. Soc.* **2016**, *138*, 1106–1109.
- (20) Gross, L.; Mohn, F.; Moll, N.; Liljeroth, P.; Meyer, G. The Chemical Structure of a Molecule Resolved by Atomic Force Microscopy. *Science* **2009**, *325*, 1110–1114.
- (21) Gross, L.; Mohn, F.; Moll, N.; Meyer, G.; Ebel, R.; Abdel-Mageed, W. M.; Jaspars, M. Organic Structure Determination Using Atomic-Resolution Scanning Probe Microscopy. *Nat. Chem.* **2010**, *2*, 821–825.
- (22) Cai, L.; Yu, X.; Liu, M.; Sun, Q.; Bao, M.; Zha, Z.; Pan, J.; Ma, H.; Ju, H.; Hu, S.; Xu, L.; Zou, J.; Yuan, C.; Jacob, T.; Björk, J.; Zhu, J.; Qiu, X.; Xu, W. Direct Formation of C-C Double-Bonded Structural Motifs by On-Surface Dehalogenative Homocoupling of *gem*-Dibromomethyl Molecules. *ACS Nano* **2018**, *12*, 7959–7966.
- (23) de Oteyza, D. G.; Gorman, P.; Chen, Y.-C.; Wickenburg, S.; Riss, A.; Mowbray, D. J.; Etkin, G.; Pedramrazi, Z.; Tsai, H.-Z.; Rubio, A.; Crommie, M. F.; Fischer, F. R. Direct Imaging of Covalent Bond Structure in Single-Molecule Chemical Reactions. *Science* **2013**, *340*, 1434–1437.
- (24) Sun, Q.; Yu, X.; Bao, M.; Liu, M.; Pan, J.; Zha, Z.; Cai, L.; Ma, H.; Yuan, C.; Qiu, X.; Xu, W. Direct Formation of C-C Triple-Bonded Structural Motifs by On-Surface Dehalogenative Homocouplings of Tribromomethyl-Substituted Arenes. *Angew. Chem., Int. Ed.* **2018**, *57*, 4035–4038.
- (25) Sun, Q.; Tran, B. V.; Cai, L.; Ma, H.; Yu, X.; Yuan, C.; Stöhr, M.; Xu, W. On-Surface Formation of Cumulene by Dehalogenative Homocoupling of Alkenyl *gem*-Dibromides. *Angew. Chem., Int. Ed.* **2017**, *56*, 12165–12169.
- (26) Pavliček, N.; Schuler, B.; Collazos, S.; Moll, N.; Pérez, D.; Guitián, E.; Meyer, G.; Peña, D.; Gross, L. On-Surface Generation and Imaging of Arynes by Atomic Force Microscopy. *Nat. Chem.* **2015**, *7*, 623–628.
- (27) Pavliček, N.; Gawel, P.; Kohn, D. R.; Majzik, Z.; Xiong, Y.; Meyer, G.; Anderson, H. L.; Gross, L. Polyene Formation *via* Skeletal Rearrangement Induced by Atomic Manipulation. *Nat. Chem.* **2018**, *10*, 853–858.
- (28) Kaiser, K.; Scriven, L. M.; Schulz, F.; Gawel, P.; Gross, L.; Anderson, H. L. An *sp*-Hybridized Molecular Carbon Allotrope, Cyclo[18]carbon. *Science* **2019**, *365*, 1299–1301.
- (29) Alemani, M.; Peters, M. V.; Hecht, S.; Rieder, K.-H.; Moresco, F.; Grill, L. Electric Field-Induced Isomerization of Azobenzene by STM. *J. Am. Chem. Soc.* **2006**, *128*, 14446–14447.
- (30) Ho, C.-L.; Yu, Z.-Q.; Wong, W.-Y. Multifunctional Poly-metallaynes: Properties. *Chem. Soc. Rev.* **2016**, *45*, 5264–5295.
- (31) Springborg, M. Quasi-One-Dimensional Materials: Polymers and Chains. *J. Solid State Chem.* **2003**, *176*, 311–318.
- (32) Liu, J.; Chen, Q.; Xiao, L.; Shang, J.; Zhou, X.; Zhang, Y.; Wang, Y.; Shao, X.; Li, J.; Chen, W.; Xu, G.; Tang, H.; Zhao, D.; Wu, K. Lattice-Directed Formation of Covalent and Organometallic Molecular Wires by Terminal Alkynes on Ag Surfaces. *ACS Nano* **2015**, *9*, 6305–6314.
- (33) Sun, Q.; Cai, L.; Ma, H.; Yuan, C.; Xu, W. Dehalogenative Homocoupling of Terminal Alkynyl Bromides on Au(111): Incorporation of Acetylenic Scaffolding into Surface Nanostructures. *ACS Nano* **2016**, *10*, 7023–7030.
- (34) Pham, T. A.; Tran, B. V.; Nguyen, M.-T.; Stöhr, M. Chiral-Selective Formation of 1D Polymers Based on Ullmann-Type Coupling: The Role of the Metallic Substrate. *Small* **2017**, *13*, 1603675.
- (35) Liu, M.; Li, S.; Zhou, J.; Zha, Z.; Pan, J.; Li, X.; Zhang, J.; Liu, Z.; Li, Y.; Qiu, X. High-Yield Formation of Graphdiyne Macrocycles through On-Surface Assembling and Coupling Reaction. *ACS Nano* **2018**, *12*, 12612–12618.
- (36) Kawai, S.; Krejčí, O.; Foster, A. S.; Pawlak, R.; Xu, F.; Peng, L.; Orita, A.; Meyer, E. Diacetylene Linked Anthracene Oligomers Synthesized by One-Shot Homocoupling of Trimethylsilyl on Cu(111). *ACS Nano* **2018**, *12*, 8791–8797.
- (37) Frank, K. G.; Selegue, J. P. Ruthenium-Tungsten and Iron-Tungsten Complexes with Ethynyl and Ethynediyl Bridges. *J. Am. Chem. Soc.* **1990**, *112*, 6414–6416.